# Indium surfactant assisted molecular beam epitaxy of AlScN

Cite as: APL Mater. 13, 101103 (2025); doi: 10.1063/5.0276421
Submitted: 17 April 2025 • Accepted: 18 September 2025 •
Published Online: 3 October 2025



Pierce Lonergan,[1,a)] Thai-Son Nguyen,[2] Chandrashekhar Savant,[2] Henryk Turski,[1,3] Huili Grace Xing,[1,2,4] and Debdeep Jena[1,2,4,5]

## AFFILIATIONS

[1] School of Electrical and Computer Engineering, Cornell University, Ithaca, New York 14853, USA
[2] Department of Materials Science and Engineering, Cornell University, Ithaca, New York 14853, USA
[3] Institute of High Pressure Physics, Polish Academy of Sciences, Sokołowska 29/37, Warsaw 01-142, Poland
[4] Kavli Institute at Cornell for Nanoscale Science, Cornell University, Ithaca, New York 14853, USA
[5] School of Applied and Engineering Physics, Cornell University, Ithaca, New York 14853, USA

[a)] **Author to whom correspondence should be addressed:** pal245@cornell.edu

## ABSTRACT

The epitaxial growth of AlScN on GaN has been traditionally performed in the nitrogen-rich condition because growth in metal-rich conditions results in the formation of Al–Sc intermetallic precipitates. Nitrogen-rich growth conditions promote island formation and roughen the surface, which is typically avoided in metal-rich growth conditions. In this work, we identify a wide window of practical growth conditions for AlScN/GaN heterostructures in which the use of indium during the growth of the AlScN layers helps mimic metal-rich growth conditions while preventing the incorporation of indium into the AlScN epitaxial layer. As a result of indium acting as a surfactant, AlScN surfaces with rms roughness as low as 0.36 nm and exhibiting step morphology are observed. We find that the growth of AlScN outside this surfactant-window results in indium incorporation at low growth temperatures or pit formation at high indium fluxes. These findings provide an alternative growth technique for highly crystalline AlScN/GaN heterostructures that overcomes limitations of nitrogen-rich growth conditions by using indium as a surfactant.





AlScN is a promising material with a plethora of applications in GaN high-electron-mobility transistors (HEMTs)/ferroelectric high-electron-mobility transistors (FerroHEMTs), bulk acoustic wave (BAW) resonators, visible and UV lasers, and quantum photonics due to its strong piezoelectric behavior, high-K dielectric, ferroelectric nature, and nonlinear optical properties.[1–7] In particular, when compared to AlN, wurtzite AlScN has a 3 times higher electromechanical coupling coefficient, 5 times higher second-harmonic generation, and a higher $d_{33}$ piezoelectric coefficient that increases with scandium content.[1–4] Plus, AlScN can be lattice-matched to GaN at 9%–11% mole fraction of Sc, which enables the design of strain-free layers on GaN-based platforms with high-crystalline quality films.[8,9] Coupled with the fact that the growth condition of AlScN is compatible with that of GaN, AlScN offers unique advantages compared to AlGaN and AlInN used in GaN based devices.[10] Thus, it is of great importance to find techniques to help optimize the surface morphology and growth mode of AlScN.

To date, in molecular beam epitaxy, AlScN is grown mainly under nitrogen-rich (N-rich) conditions to promote the incorporation of Sc in nitrided form, to ensure wurtzite phase purity, and to prevent the unfavorable formation of Al–Sc intermetallics under metal-rich conditions.[10,11] This is in contrast to the growth of most III-nitrides and their alloys, such as GaN, InN, AlN, AlGaN, GaScN, etc., which are obtained in high crystallinity and phase purity in metal-rich conditions.[12] The reason for the dissimilarity in these growth conditions lies in the differences in bonding strength to N with Al > Sc > Ga > In.[13–15] N has a higher thermodynamic preference to bond to Al than to Sc. Under metal-rich conditions, the Al preferentially replaces the Sc cation in the Sc–N bond, resulting in excess Sc on the surface.[11,13] Instead of desorbing, the Sc reacts

with Al to produce Al–Sc intermetallics. Thus, to incorporate the Sc to form AlScN, nitrogen-rich growth conditions are required. In GaScN, the Sc replaces the Ga cation in the Ga–N bond, resulting in excess Ga on the surface that acts as a surfactant during the growth.[12]

N-rich growth conditions present their own challenges, such as growth by 3D nucleation islands that often result in the suppression of underlying morphologies and the formation of rougher material surfaces.[16] Indium has been used as a surfactant in the synthesis of other materials, such as AlGaN, where it acts to promote 2D step flow growth.[17] For Al and Ga, In can lower the Ehrlich–Schwoebel barrier[18] and promote the descent of Al and Ga atoms down atomic steps.[17] In addition, In helps to temporarily occupy energetically favorable lattice sites to then exchange with another Al or Ga atom, which aids in the lowering of pit formations on the surface.[17] The exchange process is due to the Ga–N and Al–N bonds (2.45 and 2.74 eV, respectively) being more favorable than the In–N bond (2.08 eV).[13,14] In the case of AlScN, the bond strength of Al–N and Sc–N (2.72 eV) is considerably stronger than that for both Ga–N and In–N, resulting in preferential incorporation of Al and Sc over In and Ga. This means In and Ga both have the potential of being surfactants in the growth of AlScN.[13,15]

However, AlScN is typically grown at substrate temperatures between 500 and 800 °C.[11,19,20] For example, Hardy *et al.* report that increasing the growth temperature from 520 to 815 °C results in a degradation of the crystal quality of AlScN as reflected in an increase in the x-ray $\omega$ FWHM from 265 arcsec (~ 0.074°) to greater than 750 arcsec (~ 0.208°).[11] At lower temperatures, the reflection high-energy electron diffraction (RHEED) pattern for AlScN becomes spotty.[11] The degradation in the phase purity of AlScN results in worse material properties, such as a reduction in the piezoelectric response.[19] At the conventional substrate temperatures of AlScN, Ga has a much slower desorption rate than In[21] and can be incorporated into AlScN to form a quaternary alloy.[22] Combined with the fact that AlScN is grown in N-rich conditions, Ga will behave more as an incorporating atom than a surfactant. Thus, In would appear to be a better solution as a surfactant. In this work, we investigate the impact of the presence of In on the growth of AlScN and identify the growth conditions appropriate for surfactant-assisted, smooth surface morphologies.

All AlScN samples in this work were grown by plasma-assisted molecular beam epitaxy using a Veeco Gen10 MBE reactor on *c*-plane, Ga-polar bulk semi-insulating GaN substrates. The growth surface of the films was monitored *in situ* using a kSA Instruments RHEED paired with a Staib electron gun operated at 14.5 kV, 1.45 A. The nitrogen was provided using a RF plasma source with a flow rate of 1.05 sccm and 200 W RF power. Scandium, aluminum, indium, and gallium were supplied using separate effusion cells. Before the growth of AlScN films, a 100 nm unintentionally doped (UID) GaN buffer layer was grown under metal-rich conditions at a substrate temperature measured by a thermocouple ($T_C$) of 650 °C, following a Ga polish of the underlying substrate at 750 °C. Excess Ga was fully consumed by exposing the surface to reactive $N_2$ before the subsequent growth of the AlScN layer, as confirmed by monitoring RHEED. The AlScN films were all grown using a (Sc + Al)/N ratio of 0.7, similar to previous reports.[3,8] In addition, the Al + Sc metal flux was $1.3 \times 10^{-7}$ Torr (2.28 nm/min) for all samples.

The surface morphology was measured *ex situ* with an Asylum Research Cypher ES atomic force microscope (AFM). The crystal structure and thickness of the AlScN films were determined by x-ray diffraction (XRD) and x-ray reflectivity (XRR). In addition, XRD was used to check for peaks at ~ 17.55° and ~ 18.40°, which would indicate the unfavorable formation of rock salt ScN and intermetallic $Al_3Sc$, respectively.[11] XRD and XRR were collected with a PANalytical Empyrean system with Cu K$\alpha$1 radiation. The chemical composition of the AlScN films was measured by energy-dispersive x-ray spectroscopy (EDAX) using a Zeiss LEO 1550 FESEM equipped with a Bruker energy-dispersive x-ray spectroscopy silicon drift detector (SDD). The chemical composition was also measured by x-ray photoelectron spectroscopy (XPS) using a ThermoFisher Scientific Nexsa G2 Surface Analysis System. Room-temperature Hall-effect measurements were performed with a Nanometrics Hall system using van der Pauw geometry.

Following the same technique introduced by Heying *et al.* and measuring the Ga desorption curve on bulk GaN substrates in our growth system, we find that the substrate surface temperature $T_S$ is related to $T_C$ by the relation $T_S = T_C - 101$ °C.[21] Table I summarizes the samples used in the study. To investigate the effect of In as a surfactant, a series of AlScN samples (A, B, C, and D) was grown under varying In fluxes (0, $0.5 \times 10^{-7}$, $1.0 \times 10^{-7}$, and $6.0 \times 10^{-7}$ Torr). $T_C$ was kept constant at 650 °C, as this is a compatible growth temperature with GaN for future integration. A temperature series was also carried out using the intermediate In flux of $1.0 \times 10^{-7}$ Torr, which yielded the smoothest surface morphology at 650 °C. The $T_C$ values used were 450, 550, 650, and 750 °C to give the samples E, F, C, and G, respectively.

**TABLE I.** Growth parameters (in flux and $T_C$), EDAX/XPS chemical concentration of Al, Sc, and In, AFM RMS, growth rate, and 002 XRD peak position for all samples.

| Sample ID | In flux ($10^{-7}$ Torr) | $T_C$ (°C) | EDAX/XPS Al (at. %) | EDAX/XPS Sc (at. %) | EDAX/XPS In(at. %) | AFM RMS (nm) | Growth rate (nm/min) | 002 peak $\omega$ (°) |
|---|---|---|---|---|---|---|---|---|
| A | 0.0 | 650 | 92.5/93.0 | 7.06/5.86 | 0.052/0.24 | 0.46 | 2.28 | 18.07 |
| B | 0.5 | 650 | 92.7/92.7 | 6.97/7.05 | 0.027/0.21 | 0.471 | 2.32 | 18.06 |
| C | 1.0 | 650 | 92.4/93.0 | 6.56/5.56 | 0.055/0.46 | 0.445 | 2.30 | 18.07 |
| D | 5.0 | 650 | 92.3/90.8 | 7.56/8.14 | 0.13/1.05 | 0.846 | 2.38 | 18.03 |
| E | 1.0 | 750 | 92.3/90.8 | 7.86/7.31 | 0.091/0.12 | 0.361 | 2.30 | 18.08 |
| F | 1.0 | 550 | 88.2/80.2 | 6.34/5.76 | 5.41/14.21 | 9.053 | 2.55 | 17.96 |
| G | 1.0 | 450 | 83.5/65.8 | 6.63/7.47 | 9.86/30.8 | 0.502 | 2.77 | 17.69 |

First, we investigated the effect of different In fluxes on AlScN growth at $T_C$ = 650 °C. Figure 1(a) shows the schematic layer structure of the grown heterostructure for all samples. The heterostructure is 100 nm of UID GaN followed by 100 nm of AlScN. Figure 1(b) shows a 5 × 5 $\mu m^2$ AFM micrograph of the underlying UID GaN buffer layer with RMS roughness = 0.370 nm. Atomic steps are present on the GaN buffer layer as characteristic of a metal-rich growth, while the "hills" morphology is carried over from the underlying substrate. Figures 1(c)–1(f) show the corresponding 5 × 5 $\mu m^2$ AFM micrographs and RHEED patterns of the AlScN layers grown with different In fluxes. Figure 1(c) shows the 5 × 5 $\mu m^2$ AFM micrograph of the 0.0 Torr In flux control sample (sample A) with a RMS roughness of 0.460 nm. Unsurprisingly, the sample shows suppression of the underlying UID GaN morphology and 3D islands scattered throughout the surface, which is typical for 3D growth modes due to N-rich growth conditions. The corresponding RHEED shows a spotty pattern due to the formation of islands during growth.

However, for sample B, where the In flux was increased to 0.5 × $10^{-7}$ Torr, the AFM in Fig. 1(d), having an RMS roughness of 0.471 nm, shows a different story. Unlike sample A, sample B shows a morphology nearly identical to that of the underlying UID GaN buffer layer with the same characteristic "hills" found on the GaN substrate (not shown), even after 100 nm of AlScN, suggesting a suppression of island growth. The RHEED in Fig. 1(d) for sample B exhibits a transition from the spotty RHEED pattern seen for sample A to a much streakier pattern with spots centered in the streaks. This strongly indicates a blend between a Volmer–Weber (3D) and a Frank–van der Merwe (2D) growth mode.[23,24]

The AFM and RHEED in Fig. 1(e) for sample C show similar behavior to that of sample B. The RHEED is streaky with spots centered in the streak, and the AFM shows the UID GaN surface morphology being carried over. The large 3D nucleation islands are suppressed, and surface pits are absent. The two differences between samples B and C are that the latter shows a stronger ordering of surface features and a lower RMS roughness at 0.445 nm.

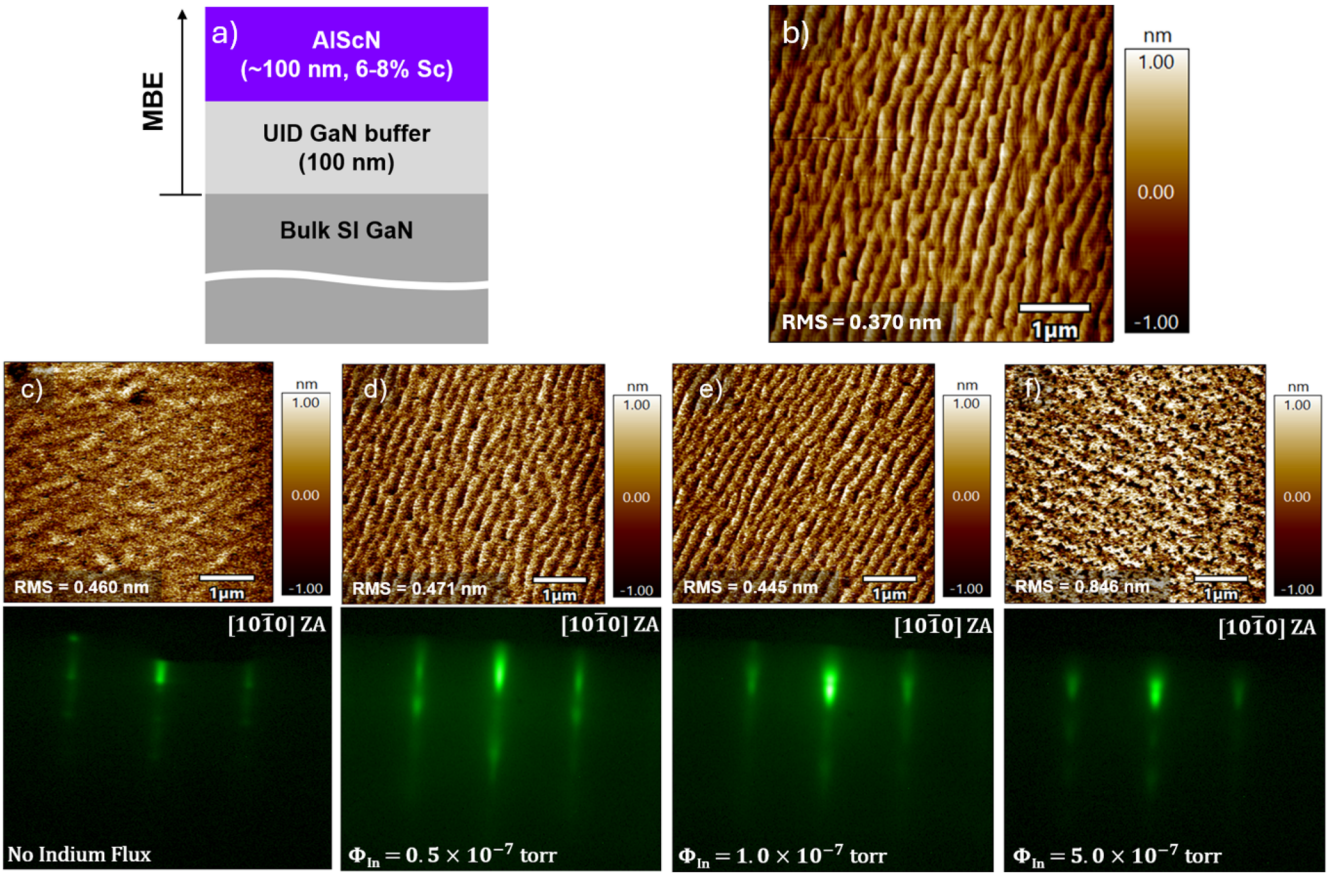


**FIG. 1.** (a) Heterostructure schematics of the AlScN/GaN. (b) 5 × 5 $\mu m^2$ AFM micrograph of the underlying UID GaN buffer with an RMS = 0.370 nm. (c) 5 × 5 $\mu m^2$ AFM micrograph (RMS = 0.460 nm) of sample A showing suppression of the underlying UID GaN morphology and *in situ* RHEED showing a spotty pattern characteristic of 3D island dominated growth. (d) 5 × 5 $\mu m^2$ AFM micrograph (RMS = 0.471 nm) of sample B showing continuity of the underlying UID GaN morphology, and *in situ* RHEED showing a streaky pattern with small spots within the streaks. (e) 5 × 5 $\mu m^2$ AFM micrograph (RMS roughness = 0.445 nm) of sample E showing continuity of the underlying UID GaN morphology, and *in situ* RHEED showing a streaky pattern with small spots within the streaks, much like the 0.5 × $10^{-7}$ Torr sample. (f) 5 × 5 $\mu m^2$ AFM micrograph (RMS = 0.846 nm) of sample F showing a high pit density, and *in situ* RHEED showing a spotty pattern.

The suppression of granular morphology, 3D island growth, and pit formation is partly due to the enhancement of the surface diffusion length for Al and Sc adatoms, thanks to the presence of In.[25] When the In flux was increased to $5.0 \times 10^{-7}$ Torr (sample D), the benefits of the surfactant disappeared. As shown in Fig. 1(f), the AFM for sample D shows an increase in surface RMS roughness to 0.846 nm and the formation of a high pit density. Similar pit formation due to excessive In flux has been seen in both In being used as a surfactant for GaN growth and the growth of AlScInN/GaN heterostructures.[25,26] The large pit formation is likely due to a reduction in the surface diffusion length resulting from too much In impinging on the surface. The RHEED diffraction spots corresponding to the twin-cubic rock-salt phase (ScN) were not observed in the RHEED patterns for all the samples used in the In flux series.[27]

To assess whether the In is acting as a surfactant or as an incorporating atom, chemical and structural analysis through x-ray techniques was performed. These specific methodologies were chosen since In incorporation will result in a change in lattice constants, growth rates, surface chemistry, and bulk composition measured by using XRD, XRR, XPS, and EDAX, respectively. In Fig. 2(a), the 002 Bragg reflections for both GaN and AlScN are seen with Pendellösung fringes surrounding the AlScN peak, indicating a sharp interface. For the In flux series, the ScN and $Al_3Sc$ peaks are absent in the collected XRD pattern, indicating the lack of formation for either phase. The suppression of the undesirable phases is further supported by RHEED patterns in Figs. 1(c)–1(f) lacking the diffraction spots corresponding to the twin-cubic rock-salt (ScN) phase.[27] The 002 AlScN peaks are at 18.07°, 18.06°, 18.07°, and 18.03° for samples A, B, C, and D, respectively. The insignificant shift of the AlScN 002 Bragg reflections suggests little to no indium incorporation into wurtzite AlScN films.

The growth rates for each film were found by XRR as another way of evaluating In incorporation. The incorporation of In into AlScN in the N-rich condition would result in an increase in the

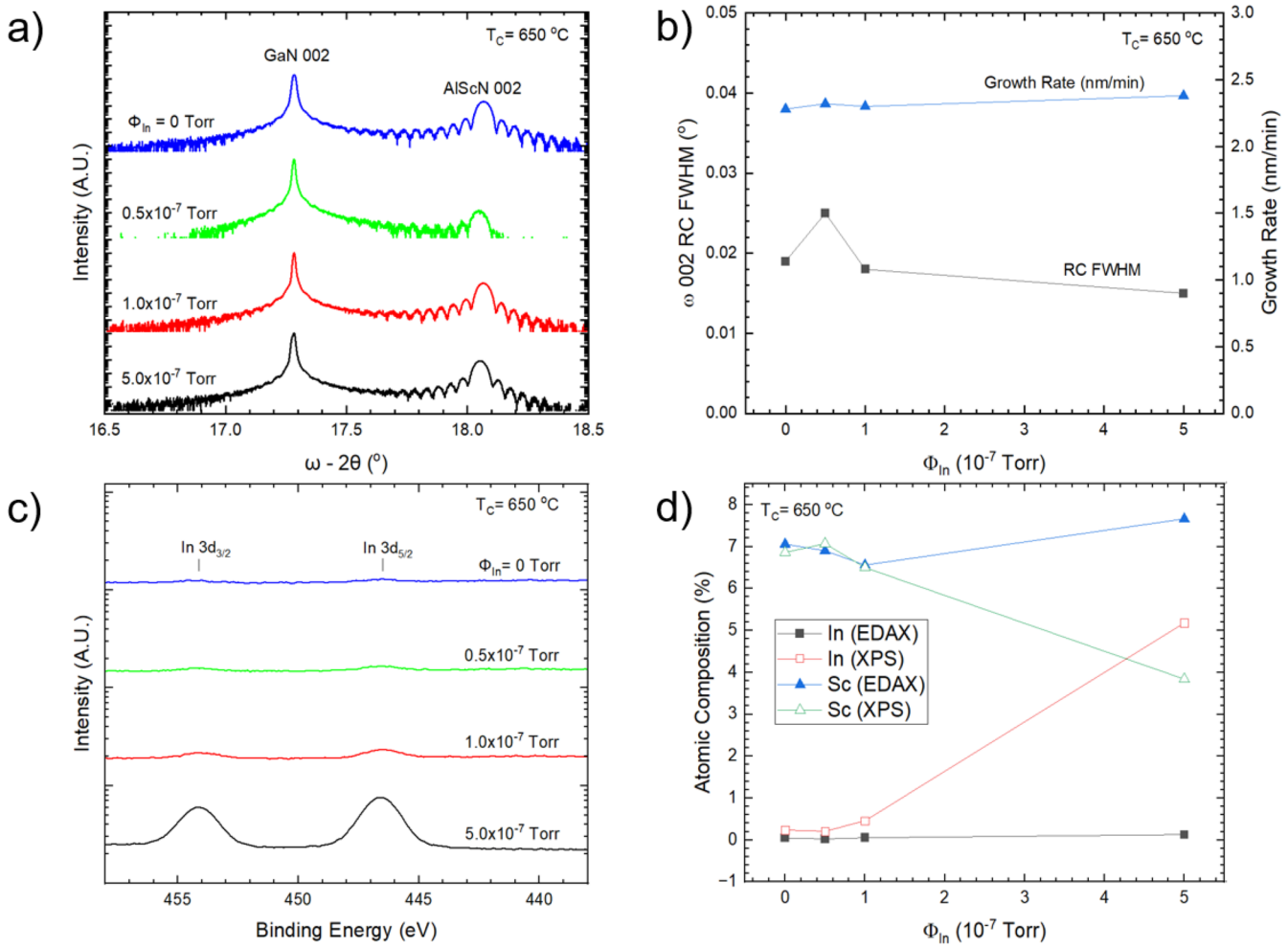


**FIG. 2.** (a) Symmetric $2\theta$–$\omega$ XRD of the 002 peak for both GaN and AlScN for the In flux series. (b) Full-width at half maximum (FWHM) for the 002 rocking curve (RC) and growth rate as a function of the In flux to assess defect density and possible In incorporation, respectively. (c) XPS scan of the In3d$_{5/2}$ and In3d$_{3/2}$ peaks to assess the incorporation of In for the In flux series. (d) Atomic composition for both In and Sc found by XPS and EDAX as a function of the indium flux.

growth rate. Displayed in Fig. 2(b), the growth rates measured are 2.28, 2.32, 2.30, and 2.38 nm/min for samples A, B, C, and D, respectively. The near constant growth rate, barring sample D, confirms that the In acts as a surfactant.

XPS scans for the $In3d_{5/2}$ and $In3d_{3/2}$ peaks are shown in Fig. 2(c). Based on the spectrum, only sample D showed a strong In presence on the surface. Finally, in Fig. 2(d), the compositions for both Sc and In collected from XPS and EDAX were compared. The In compositions for EDAX/XPS are 0.052/0.24%, 0.027/0.055%, 0.055/0.46%, and 0.129/5.18% for samples A, B, C, and D, respectively. For both XPS and EDAX, the In composition was near the noise floor for all samples except sample D. For the Sc compositions, the EDAX/XPS gives 7.06/6.86%, 6.90/7.07%, 6.56/6.50%, and 7.66/3.86% for samples A, B, C, and D, respectively. The result indicates that as we add more In flux, there is a higher probability of the In atoms reacting with $N^*$ species to incorporate into AlScN.

Oddly, the In composition in the bulk measured from EDAX (0.129%) for sample D is much smaller than the surface concentration found by XPS (5.18%). One possible explanation is the formation of In droplets that would alter the In content reading from XPS, but there were no In droplets seen on the surface by an optical microscope or AFM. This would mean the In is preferentially incorporated at the surface over the bulk. This is likely due to the In being displaced by either Al or Sc during the growth. The XRD peak position of sample D, being nearly identical to the other three samples, supports the idea of preferential In incorporation at the surface.

Surfactants can help lower defect density in epitaxial films grown by molecular beam epitaxy. Three examples are Au being used in homoepitaxial growth of Si on (111) Si substrates,[28] In as a surfactant in the growth of GaN to directly target stacking faults,[29] and Sb-assisted growth of InGaAs/GaAs quantum wells for improved light intensity emission.[30] As shown in Fig. 2(b), the FWHM of the symmetric rocking curve was obtained by an $\omega$ scan about the 002 axis to assess the defect density of the AlScN films. The FWHM is relatively constant across all samples at ~68.4 arcsec (0.019°), indicating little change in this structural parameter of the AlScN films grown with different In fluxes. The FWHM of the bulk GaN substrate is ~36.0 arcsec (0.010°), which helps to explain the narrow FWHM of the samples.

Based on the In flux series results, an In flux of $1.0 \times 10^{-7}$ Torr was chosen in the subsequent temperature series, as this flux gave the lowest surface roughness (0.471 nm) and an ordered surface morphology. The chosen $T_C$s were 450, 550, 650, and 750 °C. In Fig. 3(a), the AFM for sample E grown at 750 °C provided the lowest surface roughness (0.361 nm) as well as the best suppression of island formations and continuity of the underlying UID GaN. The surface diffusion of adatoms is increased at higher growth temperatures, which explains why sample E gave the smoothest surface.[31] The AFM of sample C (RMS roughness = 0.471 nm) in Fig. 3(b) shows a morphology nearly identical to that of the underlying UID GaN buffer, with the "hills" found on the GaN buffer layer being found on the surface of the AlScN. The RHEED patterns for samples E and C, shown in Figs. 3(a) and 3(b), respectively, again show spot-modulated streaks. As discussed before in the In flux series, this is likely a competition between a Frank–van der Merwe (2D) and Volmer–Weber (3D) growth mode.[23,24] The major difference between samples E and C is that the former has more ordered features and a smoother, less granulated overall surface.

Interestingly, for sample F grown at 550 °C, the AFM in Fig. 3(c) showed the formation of islands scattered about the surface. These islands, also seen under an optical microscope, were initially thought to be In droplets. This hypothesis was proven to be incorrect after leaving the sample in dilute hydrochloric acid, which would etch the In droplets away, and redoing the AFM measurement,



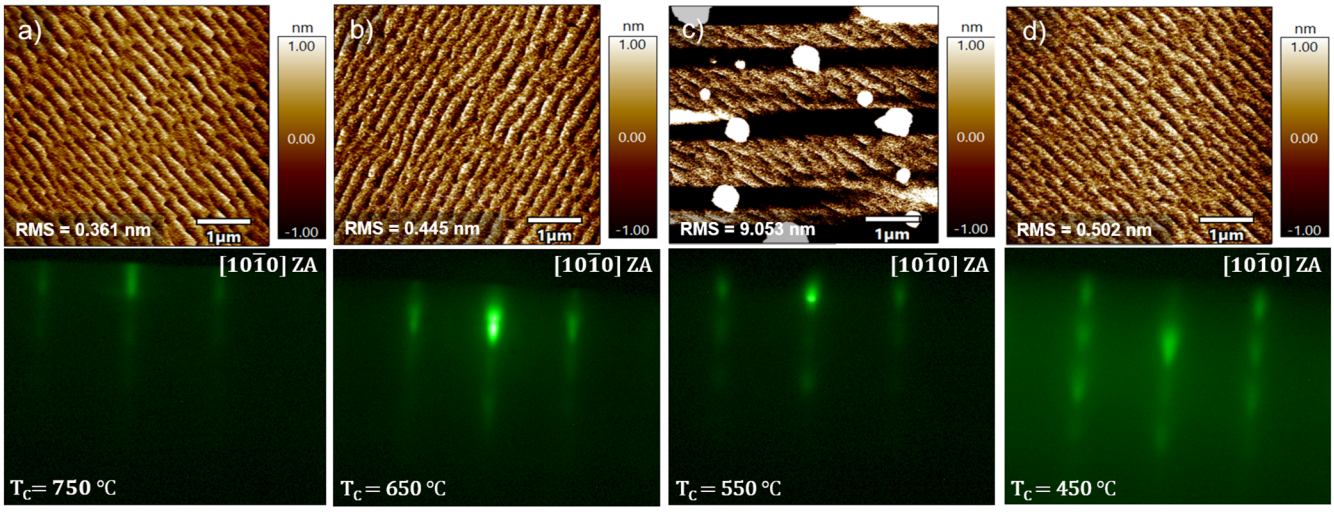


**FIG. 3.** (a) 5 × 5 $\mu m^2$ AFM micrograph (RMS roughness = 0.361 nm) of sample E showing continuity of the underlying UID GaN morphology, and *in situ* RHEED showing a pattern with small spots within the streaks. (b) 5 × 5 $\mu m^2$ AFM micrograph (RMS roughness = 0.471 nm) and *in situ* RHEED of sample C showing similar results as the 750 °C sample. (c) 5 × 5 $\mu m^2$ AFM micrograph (RMS roughness = 9.053 nm) of sample F showing significant phase separation, and *in situ* RHEED showing a spotty pattern. (d) 5 × 5 $\mu m^2$ AFM micrograph (RMS roughness = 0.502 nm) and *in situ* RHEED of sample G reverting back to the same behavior as the 750 and 650 °C samples.

giving the result in Fig. 3(c). This phenomenon is repeatable for the same In flux and growth temperature and is discussed later. Furthermore, the RHEED pattern shown in Fig. 3(c) has more discrete spots compared to other RHEED patterns in this series. However, for sample G grown at 450 °C, the islands disappeared, the surface returned to showing a continuation of the underlying UID GaN surface morphology, and the RHEED once again had a streaky pattern with dots inserted in the streaks. Just as in the In flux series, the RHEED diffraction spots corresponding to the twin-cubic rock-salt ScN phase were not observed for any samples in the $T_C$ series.[27] For a given In flux, increasing the temperature has a general trend of lowering the surface granularity and smoothing out the surface, excluding sample F.[31]

Just as was done for the In flux series, XPS, EDAX, XRD, and XRR were performed to study the possible In incorporation in the AlScN films. In Fig. 4(a), the 002 Bragg reflections for AlScN are shown with Pendellösung fringes present for samples E and C grown at 750 and 650 °C, respectively, indicating a sharp AlScN/GaN interface. For samples E (750 °C) and C (650 °C), they both show a near-constant 002 peak position for AlScN (18.06° and 18.07°, respectively) when compared to the control sample A (18.07°) from the In flux series. This strongly indicates little to no In incorporation in the samples grown at $T_C \geq 650$ °C. For samples F and G, there is a drastic shift in the 002 peak toward lower $2\theta$ values, indicating In incorporation to form AlScInN, which led to an increase in the *c*-lattice parameter of the unit cell due to In being a larger atom than Al and Sc. The new peak positions are 17.96 °C for sample F, grown at 550 °C , and 17.69 °C for sample G, grown at 450 °C. Interestingly, an additional side peak on the primary 002 Bragg reflection appears for sample F, indicating a possible secondary phase or wurtzite phase

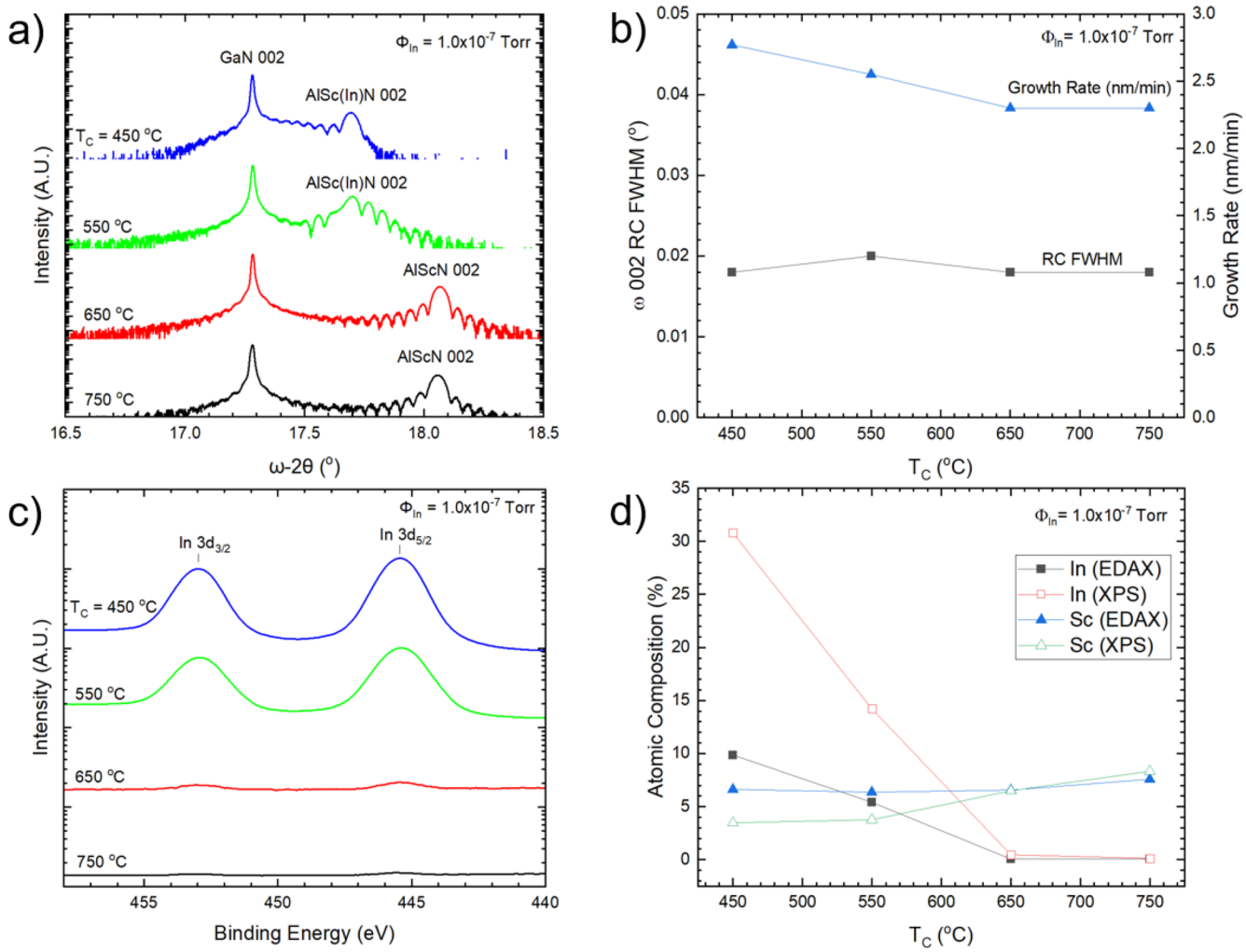


**FIG. 4.** (a) Symmetric $2\theta$–$\omega$ XRD of the 002 peak for both GaN and AlScN for the $T_C$ series. (b) Full-width half max (FWHM) for the 002 rocking curve (RC) and growth rate as a function of $T_C$ to assess defect density and possible In incorporation, respectively. (c) XPS scan of the In3d$_{5/2}$ and In3d$_{3/2}$ peaks to assess the incorporation of In for the $T_C$ series. (d) Atomic composition for both In and Sc found by XPS and EDAX as a function of $T_C$.

separation of another AlScInN composition with different In content. Furthermore, just as was true for the In flux series, the ScN and $Al_3Sc$ peaks are absent in the collected XRD pattern, indicating a suppression of undesirable phases. The suppression of the ScN and $Al_3Sc$ phase is further supported by RHEED patterns in Figs. 1(c)–1(f) lacking the diffraction spots corresponding to the twin-cubic rock-salt (ScN) phase.[27]

Moving to Fig. 4(b), at and above a $T_C$ of 650 °C, there is a relatively constant growth rate of 2.30 nm/min that is nearly equal in value to the growth rate of control sample A (2.28 nm/min), indicating a lack of In incorporation again. However, for the samples grown below 650 °C, there is an increase in growth rate to 2.55 and 2.77 nm/min for samples F and G, respectively, indicating an increasing effect of In incorporation.

In Fig. 4(b), the FWHM was relatively constant across all samples at ~64.8 arcsec (0.018°). Thus, the defect density did not change with $T_C$ at a constant given flux of $1.0 \times 10^{-7}$ Torr. Interestingly, AFM morphology and XRD rocking curve FWHM for sample G were comparable to those of samples C and E, which implies that the overall crystal quality of the quaternary alloy AlSc(In)N is similar to that of AlScN with indium surfactant. Just like the indium flux series, the narrow FWHM of the samples is in part due to the bulk GaN substrate grown on, which possesses a FWHM of ~36.0 arcsec (0.010°).

Figure 4(c) shows that samples E and C have a near noise floor level of In as indicated by the absence of $In3d_{5/2}$ and $In3d_{3/2}$ peaks. However, the samples grown at $T_C < 650$ °C (F and G) have a strong peak intensity for $In3d_{5/2}$ and $In3d_{3/2}$ peaks, suggesting incorporation of In in the AlScN layer. Finally, in Fig. 4(d), the Sc compositions found by XPS/EDAX are 7.58/8.33%, 6.56/6.50%, 6.36/3.76%, and 6.63/3.47% for samples E, C, F, and G, respectively. The In composition is 0.091/0.12%, 0.055/0.46%, 5.41/14.21%, and 9.86/30.8% for samples E, C, F, and G, respectively. As shown in Fig. 4(d), the In and Sc compositions found by XPS and EDAX are in good agreement for samples grown at and above 650 °C. Although for the samples grown below 650 °C, the In and Sc compositions found by XPS and EDAX are quite different. The In composition is much higher on the surface (measured by XPS), again suggesting a preferential incorporation of In at the surface. Thus, for samples F and G, the In is no longer acting as a pure surfactant but as an incorporating atom. The additional incorporation of the In atoms for samples F and G is due to both a lower desorption rate and a lower thermal decomposition rate of the material.[32]

To investigate the possibility of phase (chemical alloy composition) separation in sample F grown at 550 °C, spot EDAX was performed using the same excitation voltage as was used for all EDAX measurements in this paper, but with the electron beam focused on an area the size of the islands in Fig. 3(c). This technique was used to measure the chemical composition of the islands in the AFM, as shown in Fig. 3(c), and the surrounding areas. The chemical composition was found to be approximately $Al_{0.78}Sc_{0.07}In_{0.15}N$ for the islands and $Al_{0.87}Sc_{0.08}In_{0.05}N$ for the area around the islands. Coupling this difference in chemical compositions on and off the island with the twin 002 peaks shown in Fig. 4(a) for sample F and the lack of etching by HCl supports the idea of phase separation. The origin of the phase separation is likely an unfavorable entropy of mixing that would induce a separation of crystal phases at this growth temperature.[33] A similar type of segregation has been observed in films such as AlInN, where InN clusters form on the surface at lower substrate temperatures around 380 °C.[34]

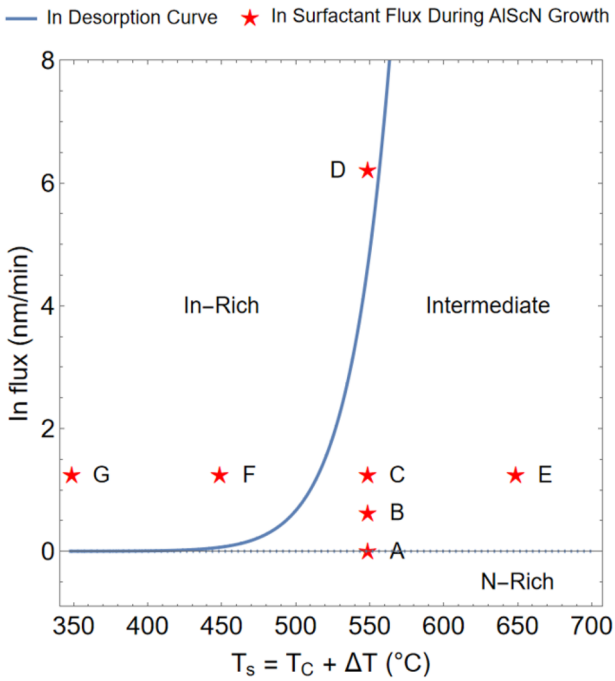


**FIG. 5.** In parameters from the study superimposed on the indium desorption plot showing the In-rich, intermediate, and N-rich regimes. Samples A, B, C, and E show no In incorporation (outside the In-rich regime), and samples D, F, and G show indium incorporation (In-rich regime). Note: $T_S$ is the calibrated temperature, and $\Delta T \sim -101$ °C.

Figure 5 shows the In surfactant fluxes and the growth temperatures used for the AlScN film samples A to G in this work, superimposed on the indium droplet desorption curve. The In droplet desorption curve was experimentally measured against the calibrated substrate temperature $T_S$. $T_S$ is related to the thermocouple measured substrate temperature $T_C$ and temperature offset $\Delta T$ by $T_S = T_C + \Delta T$. The Arrhenius fit used to give the desorption curve produced a pre-exponential coefficient of $1.24 \times 10^{14}$ nm/min. The activation energy of the In droplet desorption is 2.19 ± 0.1 eV. The reported activation energy for In desorption of InN on (0001) GaN is between 2.30 and 2.587 eV, with the In desorption activation energy over liquid In in vacuum being around 2.436 eV.[35–37] Based on the curve, samples A, B, C, and E (Table I) lie outside the In-rich region and would be expected to have little to no In incorporation in the AlScN films. Hence, the In would behave as a surfactant. In addition, samples D, F, and G (Table I) lie within the In-rich regime, meaning the films should have some level of In incorporation, with the In no longer acting as a surfactant. The chemical analysis discussed for both series agrees with the theoretical prediction from the desorption curve.

A polarization-induced 2-dimensional electron gas is expected to form at the AlScN/GaN heterojunction. However, room-temperature Hall-effect measurements for the samples in Table I were too resistive. A similar sample was subsequently grown at the optimal surfactant conditions of $T_C = 650$ °C and $\Phi_{In} = 1.0 \times 10^{-7}$

Torr, similar to sample C, with the addition of excess Ga adlayer at the AlScN/GaN interface. The Ga adlayer results from the GaN buffer layer growth.

The measured mobility at 300 K for this sample is around 285 $cm^2/V$ s with a 2DEG density of $-2.875 \times 10^{13}$ $cm^{-2}$. These values are in the expected range for mobility and 2DEG density for AlScN/GaN heterostructures without mobility-boosting AlN interlayers as reported in Ref. 8. Therefore, although In-surfactant growth does result in a sharp AlScN/GaN interface as indicated by XRD Pendellösung fringes, the mobility and 2DEG density are still heavily impacted by alloy scattering and/or the growth conditions.[38]

In point, metal-rich AlScN growths are not feasible due to the formation of Al–Sc intermetallics and degradation of the wurtzite phase purity. The conventional N-rich conditions exhibit island formation, rough surfaces, and suppression of underlying morphology. The In surfactant effect in this study has proven to be a reliable option for the growth of AlScN that avoids the formation of intermetallic phases, obtains smooth surfaces with the best RMS being 0.361 nm, and maintains the continuity of underlying morphologies. This work provides general guidelines for the ranges of In acting surfactant with higher $T_C$s (750 and 650 °C) and intermediate In fluxes ($<1.0 \times 10^{-7}$ Torr) corresponding to the best morphologies while avoiding incorporation of In atoms. At high In flux ($5.0 \times 10^{-7}$ Torr), we see In no longer acting as a surfactant but as an inhibitor to the surface diffusion of Al and Sc. In addition, at lower $T_C$s (550 and 450 °C), In begins behaving as an incorporating atom and not a pure surfactant. While both Ga and In incorporation have been used to improve the quality of AlScN films, this work shows the novelty of In in improving AlScN films without incorporation and still allowing AlScN to maintain its ternary properties.[22,25] The optimal growth regime for In as a surfactant is compatible with most AlScN epitaxial heterostructures with other III-nitrides such as AlN and GaN, providing a new pathway to the epitaxial, crystalline AlScN films with high surface quality for use in electronics, photonics, and acoustoelectric devices.[11]

See the supplementary material for the rocking curve data of the symmetric 002 peak for samples A through G, as well as the bulk GaN substrate on which the samples were grown.

This work was partially supported by the Cornell Center for Materials Research with funding from the NSF MRSEC program (Grant No. DMR-1719875). This work was supported in part by SUPREME, one of seven centers in JUMP 2.0, a Semiconductor Research Corporation (SRC) program sponsored by DARPA.

## AUTHOR DECLARATIONS

### Conflict of Interest

The authors have no conflicts to disclose.

### Author Contributions

**Pierce Lonergan**: Conceptualization (lead); Data curation (equal); Formal analysis (equal); Investigation (lead); Methodology (lead); Writing – original draft (equal); Writing – review & editing (equal). **Thai-Son Nguyen**: Conceptualization (equal); Data curation (equal); Formal analysis (equal); Investigation (equal); Methodology (equal); Writing – review & editing (equal). **Chandrashekhar Savant**: Conceptualization (equal); Data curation (equal); Formal analysis (equal); Investigation (equal); Methodology (equal); Writing – review & editing (equal). **Henryk Turski**: Conceptualization (equal); Writing – review & editing (equal). **Huili Grace Xing**: Funding acquisition (equal); Project administration (supporting); Resources (equal); Supervision (supporting). **Debdeep Jena**: Funding acquisition (lead); Project administration (lead); Resources (equal); Supervision (lead); Writing – review & editing (equal).

## DATA AVAILABILITY

The data that support the findings of this study are available from the corresponding author upon reasonable request.

## REFERENCES

[1] J. Casamento, K. Nomoto, T. S. Nguyen, H. Lee, C. Savant, L. Li, A. Hickman, T. Maeda, J. Encomendero, V. Gund, A. Lal, J. C. M. Hwang, H. G. Xing, and D. Jena, "FerroHEMTs: High-current and high-speed all-epitaxial AlScN/GaN ferroelectric transistors," in *2022 International Electron Devices Meeting (IEDM)* (IEEE, 2022); arXiv:2302.14209 [physics], pp. 11.1.1–11.1.4.

[2] K. Umeda, H. Kawai, A. Honda, M. Akiyama, T. Kato, and T. Fukura, "Piezoelectric properties of ScAlN thin films for piezo-MEMS devices," in *2013 IEEE 26th International Conference on Micro Electro Mechanical Systems (MEMS)* (IEEE, 2013), pp. 733–736.

[3] L. van Deurzen, T.-S. Nguyen, J. Casamento, H. G. Xing, and D. Jena, "Epitaxial lattice-matched AlScN/GaN distributed Bragg reflectors," Appl. Phys. Lett. **123**, 241104 (2023).

[4] J. Liu, P.-L. Thériault, S. Liu, D. Wang, W. Wu, Q. Wen, Z. Zhang, M. Soltani, M. Kira, S. Kéna-Cohen, and Z. Mi, "Second-order optical nonlinearities in ferroelectric ScAlN for quantum photonics," in *2023 IEEE Photonics Conference (IPC)* (IEEE, 2023), pp. 1–2.

[5] K. Nomoto, J. Casamento, T.-S. Nguyen, L. Li, H. Lee, C. Savant, A. L. Hickman, T. Maeda, J. Encomendero, V. Gund *et al.*, "AlScN/GaN HEMTs with 4 A/mm on-current and maximum oscillation frequency >130 GHz," Appl. Phys. Express **18**, 016506 (2025).

[6] T. Nguyen, K. Nomoto, W. Zhao, C. Savant, H. Xing, and D. Jena, "Strain-balanced AlScN/GaN HEMTs with fT/fMAX of 173/321 GHz," in *2024 IEEE International Electron Devices Meeting (IEDM)* (IEEE, 2024), pp. 1–4.

[7] J. Casamento, K. Nomoto, T.-S. Nguyen, H. Lee, C. Savant, L. Li, A. Hickman, T. Maeda, Y.-T. Shao, J. Encomendero *et al.*, "AlScN high electron mobility transistors: Integrating high piezoelectric, high k dielectric, and ferroelectric functionality," in *2023 IEEE BiCMOS and Compound Semiconductor Integrated Circuits and Technology Symposium (BCICTS)* (IEEE, 2023), pp. 132–136.

[8] T.-S. Nguyen, N. Pieczulewski, C. Savant, J. J. P. Cooper, J. Casamento, R. S. Goldman, D. A. Muller, H. G. Xing, and D. Jena, "Lattice-matched multiple channel AlScN/GaN heterostructures," APL Mater. **12**, 101117 (2024).

[9] D. V. Dinh, J. Lähnemann, L. Geelhaar, and O. Brandt, "Lattice parameters of $Sc_xAl_{1-x}N$ layers grown on GaN(0001) by plasma-assisted molecular beam epitaxy," Appl. Phys. Lett. **122**, 152103 (2023).

[10] J. Casamento, C. S. Chang, Y.-T. Shao, J. Wright, D. A. Muller, H. G. Xing, and D. Jena, "Structural and piezoelectric properties of ultra-thin $Sc_xAl_{1-x}N$ films grown on GaN by molecular beam epitaxy," Appl. Phys. Lett. **117**, 112101 (2020).

[11] M. T. Hardy, B. P. Downey, N. Nepal, D. F. Storm, D. S. Katzer, and D. J. Meyer, "Epitaxial ScAlN grown by molecular beam epitaxy on GaN and SiC substrates," Appl. Phys. Lett. **110**, 162104 (2017).

[12] H. C. L. Tsui, L. E. Goff, N. P. Barradas, E. Alves, S. Pereira, H. E. Beere, I. Farrer, C. A. Nicoll, D. A. Ritchie, and M. A. Moram, "The effect of metal-rich growth conditions on the microstructure of $Sc_xGa_{1-x}N$ films grown using molecular beam epitaxy," Phys. Status Solidi A **212**, 2837–2842 (2015).

[13] W. E. Hoke, A. Torabi, J. J. Mosca, and T. D. Kennedy, "Thermodynamic analysis of cation incorporation during molecular beam epitaxy of nitride films using

metal-rich growth conditions," J. Vac. Sci. Technol., B: Microelectron. Nanometer Struct. Proces., Meas., Phenom. **25**, 978–982 (2007).
[14]A. K. Kandalam, R. Pandey, M. A. Blanco, A. Costales, J. M. Recio, and J. M. Newsam, "First principles study of polyatomic clusters of AlN, GaN, and InN. 1. Structure, stability, vibrations, and ionization," J. Phys. Chem. B **104**, 4361–4367 (2000).
[15]F. Tientega and J. F. Harrison, "Electronic and geometric structure of the diatomics ScN, ScP and ScAs," Chem. Phys. Lett. **223**, 202–206 (1994).
[16]G. Ferro, H. Okumura, and S. Yoshida, "Growth mode of AlN epitaxial layers on 6H-SiC by plasma assisted molecular beam epitaxy," J. Cryst. Growth **209**, 415–418 (2000).
[17]H. Jia, W. Yang, X. Zhang, X. Zhou, H. Qiu, H. Qin, S. Lu, and L. Bian, "Effects and mechanisms of in surfactant on high Al-content AlGaN grown by plasma-assisted molecular beam epitaxy," Opt. Express **30**, 1782–1792 (2022).
[18]Z. Zhang and M. G. Lagally, "Atomic-scale mechanisms for surfactant-mediated layer-by-layer growth in homoepitaxy," Phys. Rev. Lett. **72**, 693–696 (1994).
[19]M. Akiyama, K. Kano, and A. Teshigahara, "Influence of growth temperature and scandium concentration on piezoelectric response of scandium aluminum nitride alloy thin films," Appl. Phys. Lett. **95**, 162107 (2009).
[20]P. Wang, D. A. Laleyan, A. Pandey, Y. Sun, and Z. Mi, "Molecular beam epitaxy and characterization of wurtzite $Sc_xAl_{1-x}N$," Appl. Phys. Lett. **116**, 151903 (2020).
[21]B. Heying, R. Averbeck, L. F. Chen, E. Haus, H. Riechert, and J. S. Speck, "Control of GaN surface morphologies using plasma-assisted molecular beam epitaxy," J. Appl. Phys. **88**, 1855–1860 (2000).
[22]S. Yang, D. Wang, M. M. H. Tanim, D. Wang, and Z. Mi, "Molecular beam epitaxy and characterization of ferroelectric quaternary alloy $Sc_{0.2}Al_{0.45}Ga_{0.35}N$," Appl. Phys. Lett. **124**, 193501 (2024).
[23]N. A. Shepelin, Z. P. Tehrani, N. Ohannessian, C. W. Schneider, D. Pergolesi, and T. Lippert, "A practical guide to pulsed laser deposition," Chem. Soc. Rev. **52**, 2294–2321 (2023).
[24]G. Le Lay and R. Kern, "Physical methods used for the characterization of modes of epitaxial growth from the vapor phase," J. Cryst. Growth **44**, 197–222 (1978).
[25]H. Ye, R. Wang, L. Yang, J. Wang, T. Wang, R. Feng, X. Xu, W. Lee, P. Wang, and X. Wang, "ScAlInN/GaN heterostructures grown by molecular beam epitaxy," Appl. Phys. Lett. **125**, 122105 (2024).
[26]K. S. Qwah, E. Farzana, A. Wissel, M. Monavarian, T. Mates, and J. S. Speck, "Indium as a surfactant: Effects on growth morphology and background impurity in GaN films grown by ammonia-assisted molecular beam epitaxy," APL Mater. **10**, 081107 (2022).
[27]C. P. Savant, A. Verma, T.-S. Nguyen, L. van Deurzen, Y.-H. Chen, Z. He, S. S. Rezaie, J. Gollwitzer, B. Gregory, S. Sarker, J. Ruff, G. Khalsa, A. Singer, D. A. Muller, H. G. Xing, D. Jena, and J. Casamento, "Self-activated epitaxial growth of ScN films from molecular nitrogen at low temperatures," APL Mater. **12**, 111108 (2024).
[28]G. D. Wilk, R. E. Martinez, J. F. Chervinsky, F. Spaepen, and J. A. Golovchenko, "Low-temperature homoepitaxial growth on Si(111) mediated by thin overlayers of Au," Appl. Phys. Lett. **65**, 866–868 (1994).
[29]W. K. Fong, C. F. Zhu, B. H. Leung, C. Surya, B. Sundaravel, E. Z. Luo, J. B. Xu, and I. H. Wilson, "Characterizations of GaN films grown with indium surfactant by RF-plasma assisted molecular beam epitaxy," Microelectron. Reliab. **42**, 1179–1184 (2002).
[30]D.-S. Jiang, Y.-H. Qu, H.-Q. Ni, D.-H. Wu, Y.-Q. Xu, and Z.-C. Niu, "Optical properties of inGaAs/GaAs quantum wells grown by Sb-assisted molecular beam epitaxy," J. Cryst. Growth **288**, 12–17 (2006), part of Special Issue: International Conference on Materials for Advanced Technologies (ICMAT 2005, Symposium M.
[31]S. Clarke and D. D. Vvedensky, "Growth mechanism for molecular-beam epitaxy of group-IV semiconductors," Phys. Rev. B **37**, 6559–6562 (1988).
[32]S. T. Liu, X. Q. Wang, G. Chen, Y. W. Zhang, L. Feng, C. C. Huang, F. J. Xu, N. Tang, L. W. Sang, M. Sumiya, and B. Shen, "Temperature-controlled epitaxy of $In_xGa_{1-x}N$ alloys and their band gap bowing," J. Appl. Phys. **110**, 113514 (2011).
[33]M. E. Twigg, S. Tomasulo, M. A. Stevens, N. A. Mahadik, N. A. Kotulak, and M. K. Yakes, "The thermodynamics and kinetics of phase separation in III–V semiconductor alloys," Thin Solid Films **793**, 140255 (2024).
[34]K. Jeganathan and M. Shimizu, "Importance of growth temperature on achieving lattice-matched and strained InAlN/GaN heterostructure by plasma-assisted molecular beam epitaxy," AIP Adv. **4**, 097113 (2014).
[35]G. Koblmüller, C. S. Gallinat, and J. S. Speck, "Surface kinetics and thermal instability of N-face InN grown by plasma-assisted molecular beam epitaxy," J. Appl. Phys. **101**, 083516 (2007).
[36]C. S. Gallinat, G. Koblmüller, J. S. Brown, and J. S. Speck, "A growth diagram for plasma-assisted molecular beam epitaxy of In-face InN," J. Appl. Phys. **102**, 064907 (2007).
[37]L. Lymperakis, K. Lymperakis, and E. Iliopoulos, "Desorption kinetics of indium adlayers on GaN(0001): Fractional order and non-monotonic behavior," J. Appl. Phys. **136**, 215701 (2024).
[38]J. Casamento, T.-S. Nguyen, Y. Cho, C. Savant, T. Vasen, S. Afroz, D. Hannan, H. G. Xing, and D. Jena, "Transport properties of polarization-induced 2D electron gases in epitaxial AlScN/GaN heterojunctions," Appl. Phys. Lett. **121**, 192101 (2022).